



**HAL**  
open science

## Non-destructive quantification of water gradient in sludge composting with Magnetic Resonance Imaging

F.P. Duval, S. Quellec, A. Trémier, C. Druilhe, François Mariette

► **To cite this version:**

F.P. Duval, S. Quellec, A. Trémier, C. Druilhe, François Mariette. Non-destructive quantification of water gradient in sludge composting with Magnetic Resonance Imaging. *Waste Management*, 2010, 30 (4), pp.610-619. 10.1016/j.wasman.2009.09.045 . hal-02593165

**HAL Id: hal-02593165**

**<https://hal.inrae.fr/hal-02593165>**

Submitted on 15 May 2020

**HAL** is a multi-disciplinary open access archive for the deposit and dissemination of scientific research documents, whether they are published or not. The documents may come from teaching and research institutions in France or abroad, or from public or private research centers.

L'archive ouverte pluridisciplinaire **HAL**, est destinée au dépôt et à la diffusion de documents scientifiques de niveau recherche, publiés ou non, émanant des établissements d'enseignement et de recherche français ou étrangers, des laboratoires publics ou privés.

1  
2  
3  
4  
5  
6  
7  
8  
9  
10  
11  
12  
13  
14  
15  
16  
17

## **Non-Destructive Quantification of Water Gradient in Sludge Composting with Magnetic Resonance Imaging**

**F.P. Duval<sup>1,3</sup>, S. Quéllec<sup>1,3</sup>, A. Trémier<sup>2,3</sup>, C. Druilhe<sup>2,3</sup>, F. Mariette<sup>1,3,\*</sup>**

1-Cemagref, UR TERE, 17 Avenue de Cucillé, CS 64427, F-35044 Rennes, France.

2-Cemagref, UR GERE, F-35044 Rennes, France.

3-Université européenne de Bretagne, France.

\* Corresponding author. Tel.: +33 2 23 48 21 21; Fax: +33 2 23 48 21 15; E-mail address:  
francois.mariette@cemagref.fr

18

19 **Abstract**

20 Sludge from a slaughterhouse wastewater plant, and mixtures of bulking agent (crushed wood  
21 pallet) and sludge were studied by Nuclear Magnetic Resonance (NMR). The NMR spin-spin  
22 relaxation ( $T_2$ ) and spin-lattice relaxation ( $T_1$ ) signals for sludge, wet crushed wood pallet and  
23 mixtures of sludge and bulking agent were decomposed into three relaxation time  
24 components. Each relaxation time component was explained by a non-homogeneous water  
25 distribution on a microscopic length scale and by the porosity of the material. For all samples,  
26 the  $T_2$  relaxation time value of each component was directly related to the dry matter content.  
27 The addition of wet crushed wood to sludge induced a decrease in the relaxation time,  
28 explained by water transfer between the sludge and the wood.

29 Magnetic Resonance Imaging (MRI) and respirometric measurements were performed on  
30 sludge and wood mixtures. MR images of the mixtures were successfully obtained at different  
31 biodegradation states. Based on specific NMR measurements in an identified area located in  
32 the MRI cells, the results showed that grey levels of MR images reflected dry matter content.  
33 This preliminary study showed that MRI would be a powerful tool to measure water  
34 distribution in sludge and bulking agent mixtures and highlights the potential of this technique  
35 to increase the understanding of sludge composting.

36

37

38

39 **Keywords:** NMR, MRI, relaxation, compost, biodegradability, moisture content, bulking  
40 agent, sludge

## 41 **1. Introduction**

42 Treatment of wastewater is an important issue in western countries and research is currently  
43 being undertaken to investigate the elimination or re-use of residual sludge at better cost,  
44 including composting of wastewater sludge. In order to do so, sludge needs to be mixed with  
45 a bulking agent which creates a porous matrix. Proportions of sludge and bulking agent are  
46 chosen so that sludge covers the bulking agent with a thin layer, and then micro-organisms in  
47 the sludge are sufficiently aerated to consume the available biodegradable organic matter.  
48 During sludge composting treatment, the active biodegradation takes place in three to four  
49 weeks, followed by several months of maturation (Gupta, 2008). Selection of an initial waste  
50 recipe with optimal physical and biochemical parameters is essential to create an environment  
51 conducive to high microbial growth and activity, and then to shorten and improve the  
52 biodegradation in the active phase (Haug, 1993; Agnew, 2003). Some of the important  
53 physical parameters for this waste recipe are water content, air porosity and specific surface  
54 area.

55 Research on composting is often focused on overall understanding of the biodegradation  
56 phenomena, i.e. on a macro-scale. All the parameters of biodegradation such as oxygen  
57 consumption, bacteria activity, porosity and moisture content are averaged, and little is known  
58 regarding the influence of local behaviour of the physical parameters on overall  
59 biodegradation. Since solid wastes are very heterogeneous, better understanding of water  
60 content, porosity and specific surface spatial distribution is needed, and Magnetic Resonance  
61 Imaging (MRI) could help to fill this gap. **Indeed, most of the common techniques to measure  
62 physical parameters can not be applied along the composting process because they are  
63 invasive or destructive. Moisture measurements need sampling and drying. Classic porosity  
64 measurement implies to fill the porous volume with a liquid (Annan, 1998), which is  
65 destructive for the sample. Pycnometry is a non destructive method but results directly depend**

66 on the applied pressure leading to the measurement of total air space (TAS) or only free air  
67 space (FAS) (Su, 2006). Measurement of the specific surface is not easier. The direct  
68 measurement technique through gaseous absorption (BET) used by Palmowski et al.  
69 (Palmowski, 2003) can only be applied after drying the waste. On the contrary, MRI is non-  
70 destructive and non-invasive and thus makes it possible to follow the evolution of samples  
71 over time. MRI is well known for its medical applications, but it has been used in other fields  
72 including the wood industry (Muller, 2002), study of bacterial chemotaxis (Sherwood, 2003;  
73 Olson, 2004), chemical engineering (Mantle, 2003), civil engineering (Faure, 2005), fluid  
74 mechanics (Bonn, 2008), pharmaceutical science (Richardson, 2005) and food science (Hills,  
75 1998; Butz, 2005). In an MRI experiment, the volume in which the signal is collected is  
76 called a voxel, and its typical order of magnitude is the cubic millimetre. Voxel intensity is a  
77 function of local proton density and of their respective spin-lattice ( $T_1$ ) and spin-spin ( $T_2$ )  
78 relaxation times. Proton density is proportional to the amount of material containing protons.  
79 In most materials, water is the main constituent related to proton density. Consequently, the  
80 grey level intensity of a voxel may be related to water content or air content (*i.e.* porosity).  
81 Indeed when the voxel size is larger than the pore size the porosity is directly related to the  
82 intensity of the MRI signal: the greater the quantity of gas, the lower the signal. This method  
83 has been used in food science to quantify the distribution of porosity during proving of dough  
84 (Grenier, 2003; Lucas, 2005). In the extreme case where the pore volume is much larger than  
85 the voxel size, the pore size can be measured. For example, air cavities have been detected  
86 and quantified in food products such as cheese (Mariette, 2004; 2006). In addition to the  
87 porous fraction, the specific surface area can be estimated if the resolution of the MR images  
88 is good enough.

89 Spin-lattice ( $T_1$ ) and spin-spin ( $T_2$ ) relaxation times are related to water content and also to  
90 material microstructure and to molecular structure (Brownstein, 1979; Belton, 1987; Hills,

91 1989b; a; Denisov, 2002). Several authors have used the  $T_2$  and  $T_1$  relaxation times as tracers  
92 of water content for the investigation of draining processes (Mariette, 2006) and rehydration  
93 processes (Ziegler, 2003).

94 The aim of this study was to evaluate the potential of the MRI technique in sludge composting  
95 to quantify the water distribution. . The first part of this report focuses on the description of  
96 the nuclear magnetic resonance (NMR) signals in sludge and in mixtures of sludge and  
97 bulking agent and their sensitivity to water content. The second part describes the preliminary  
98 results of MRI images from sludge and bulking agent mixture. The potential for determination  
99 of water content and measurement of local porosity by MRI is discussed.

100

## 101 **2. Materials and Methods**

### 102 2.1 Sludge and bulking agent

103 The sludge came from the biological activated sludge treatment of the wastewater from a  
104 slaughter-house. Iron chloride and a polymeric flocculent (PRAESTOL K133) were added to  
105 the sludge to induce flocculation and, after a decantation step, the sludge was dewatered using  
106 a press band. The collected sludge was stored frozen at  $-20^{\circ}\text{C}$  in 1kg batches. Sludge was  
107 unfrozen before each experiment, initially in a refrigerator at  $4^{\circ}\text{C}$  and then at room  
108 temperature.

109 The dry matter (DM, measured by drying at  $105^{\circ}\text{C}$  until constant weight) in the sludge was  
110 13.6% of total weight, with approximately 80% organic matter to DM. The exact quantity of  
111 living bacteria present in the sludge was unknown. Flocs of bacteria were observed using  
112 optical microscopy (data not shown). Sludges with higher dry matter content were prepared  
113 using a low pressure oven (34 Mb and  $30^{\circ}\text{C}$ ). Mixtures of sludge and bulking agent were  
114 prepared by hand mixing the sludge with crushed wood pallet as bulking agent. The size of  
115 the wood chips considered was 8 to 12 mm. Wood was stored after drying at  $80^{\circ}\text{C}$ . Different

116 samples were then studied by NMR, i.e. the sludge without bulking agent, mixtures of wood  
117 and sludge, and a rehydrated wood sample (DM 45%). Since there is water transfer between  
118 sludge and dried wood after mixing, the saturated wood sample was prepared to mimic the  
119 contribution of the re-hydrated wood fraction in the mixture.

120 A combined experiment using MRI and respirometry was set up. Two large respirometric  
121 cells were prepared with 4.5 kg of sludge (wet) mixed with 2.5 kg of wood (dry mass ratio  
122 1/4.1  $g_{DM}/g_{DM}$ ). The moisture content in both cells was approximately 56%. MRI  
123 measurements were performed at day 1, day 3 and day 27 of biodegradation. Samples were  
124 taken from these cells for NMR measurement and moisture analysis at 27 days.

125

## 126 2.2 Respirometry

127 Respirometry is a useful tool to assess microbial activity (Iannotti, 1994; Adani, 2001; Gea,  
128 2004). The respirometric apparatus used in this study consisted of a 10 L airtight cylindrical  
129 reactor made of glass. Three to four kilos of precisely weighed material were introduced into  
130 the respirometric reactor on a 3 mm round mesh grid placed 70 mm above the cell bottom. An  
131 entering air flow rate of 65 L/h (compressed air) was applied throughout the experiments.  
132 Homogeneity of aeration of the entire sample was provided by means of the rapid  
133 recirculation of the exhaust gas in the cell (360 L/h). The entering and exhaust air streams  
134 were monitored for O<sub>2</sub> content using a paramagnetic O<sub>2</sub> gas analyser (MAHAIK Technology,  
135 Germany).

136 The apparatus was monitored for **the main** environmental factors influencing microbial  
137 activity, **i.e. temperature and moisture**. As shown on **Figure 1** the temperature of samples was  
138 held constant by placing each respirometric cell in a water-bath at 40°C, which is optimal for  
139 biodegradation activity (Tremier, 2005). The inlet air was preheated to 40°C using a copper  
140 tubular coil with a diameter of 10 mm, thickness of 2 mm and length of 2 m, submerged in the

141 water-bath. The sample temperatures were monitored by means of a Pt100 temperature probe  
142 (OMNI Instrument, UK) inserted in the centre of the sample. For the moisture control, the  
143 inflowing air was saturated by bubbling through two water-filled glass bottles immersed in  
144 the water-bath. Moisture condensing in the exhaust air was collected in beakers above the  
145 water-bath to prevent its return into the sample cell and its entrance into the gas analyser.

146

147

148

### 149 2.3 NMR measurements

150 All NMR measurements were performed with a 10 MHz Minispec Mq10 (Bruker,  
151 Wissembourg, France). Typical  $90^\circ$  and  $180^\circ$  pulse durations were 14  $\mu\text{s}$  and 32  $\mu\text{s}$ ,  
152 respectively, with an 8 dB pulse attenuation. The temperature was fixed at  $20^\circ\text{C}$ . Spin-Spin  
153 relaxation time ( $T_2$ ) measurements were performed using a Carr Purcell Meiboom and Gill  
154 (CPMG) sequence (Meiboom, 1958). Three thousand consecutive echoes were recorded with  
155 a time spacing of 0.1 ms between the  $90^\circ$  and the first  $180^\circ$  pulse. Recycle delay and number  
156 of scans were 2 s and 8 s, respectively. Spin-Lattice relaxation time ( $T_1$ ) measurements were  
157 performed using a saturation recovery (SR) sequence. Times between the two  $90^\circ$  pulses were  
158 varied one hundred times from 5 ms to 2000 ms. The NMR signal was acquired 28  $\mu\text{s}$  after  
159 the second  $90^\circ$  pulse in order to detect only the longest relaxation components, *i.e.*, the water  
160 proton relaxation. Recycle delay and number of scans were 2 s and 8 s, respectively.

161

### 162 2.5 Calculation of NMR parameters

163 Relaxation curves were fitted using two different methods, the Maximum Entropy Method  
164 (MEM) (Mariette, 1996), which provides a continuous distribution of relaxation components,  
165 and the Levenberg-Marquardt algorithm, which allows discrete solution for the fitting (Table



166 Curve, Jandel) (Marquardt, 1963). Moreover, no assumptions regarding the number of  
167 relaxation times are necessary with MEM compared to the Levenberg-Marquardt algorithm  
168 method.

169 For the spin-spin relaxation decay signal, the equation used for fitting according to the  
170 Levenberg-Marquardt method was:

$$171 \quad S(t)_{CPMG} = I_1 e^{-\frac{t}{T_{21}}} + I_2 e^{-\frac{t}{T_{22}}} + I_3 e^{-\frac{t}{T_{23}}} + c \quad \text{Eq.1}$$

172 where  $S(t)_{CPMG}$  is the intensity of the total relaxation signal (a.u.),  $t$  is the time of the  
173 relaxation process (ms),  $T_{2i}$  the spin-spin relaxation time of the component  $i$  (ms) and  $I_i$  the  
174 associated signal (a.u.). A constant  $c$  was added into the model in order to take into account  
175 change in the decay baseline.

176

177 Spin-Lattice relaxation curves were fitted with the Levenberg-Marquardt algorithm with the  
178 following equation:

$$179 \quad S(t)_{SR} = I_1 (1 - \alpha e^{-\frac{t}{T_{11}}}) + I_2 (1 - \alpha e^{-\frac{t}{T_{12}}}) + I_3 (1 - \alpha e^{-\frac{t}{T_{13}}}) \quad \text{Eq.2}$$

180 where  $S(t)_{SR}$  is the intensity of the total relaxation signal (a.u.),  $t$  is the time of the relaxation  
181 process (ms),  $T_{1i}$  the spin-lattice relaxation time of the component  $i$  (ms) and  $I_i$  the associated  
182 signal (a.u.). A constant  $\alpha$  was introduced to correct for imperfections in the  $90^\circ$  pulse.

183

## 184 2.6 MRI measurements

185 A 1.5 Tesla whole body MRI scanner (Magnetom Avento Siemens, Erlangen, Germany) was  
186 used. The MR images were acquired with the standard spin echo sequence. Forty-five slices  
187 of 2 mm were recorded, the distance between the centres of two consecutive slices being 4  
188 mm. The field of view was 220 mm x 220 mm for 256 x 256 pixel sampling. Echo time ( $T_E$ ),  
189 repetition time ( $T_R$ ) and pixel bandwidth were 8 ms, 1000 ms and 395 Hz/pixel, respectively.

190 The grey level intensity  $S_{ES}$  (a.u) within a voxel with a standard spin-echo sequence was given  
191 by the equation:

$$192 \quad S_{ES} = I \left( 1 - \beta e^{-\frac{T_R}{T_1}} \right) \times e^{-\frac{T_E}{T_2}} \quad \text{Eq.3}$$

193 with I the intensity related to the relaxation times  $T_1$  and  $T_2$  of the protons in the voxel.  $\beta$  is a  
194 parameter introduced to correct for imperfections in the  $90^\circ$  pulse. This equation assumed a  
195 single proton component with a single spin-spin relaxation and a single spin-lattice relaxation.  
196 In the case of multi-exponential behaviour, the grey level intensity would be a combination of  
197 the different relaxing components for both  $T_1$  and  $T_2$ .

198

### 199 **3. Results and discussion**

#### 200 **3.1 NMR**

201 Figure 2 shows typical CPMG (a) and SR (b) signals for two wood and sludge mixtures with  
202 dry matter of 24% and 70%. CPMG signal intensities decreased throughout the acquisition  
203 time  $t$ , according to equation 1. An increase in signal intensity was obtained for SR as  
204 expected from equation 2. The effects of water content on NMR parameters can be described  
205 from the two CPMG signals. Firstly, since the initial signal intensity was proportional to the  
206 sample proton content, and because water is one of the most abundant protonic molecules in  
207 our system, this explains the reduction in signal intensity from 3.7 to 2.2 a.u. observed  
208 between the two samples. Secondly, the water relaxation time is highly sensitive to water  
209 content. Indeed,  $T_2$  relaxation was directly related to molecular mobility, i.e., the slower the  
210 molecular mobility the shorter the relaxation time (Belton, 1990). The relaxation time of a  
211 small molecule is thus always higher than the relaxation time of a large molecule. Moreover,  
212 the exchange between water protons and exchangeable protons from the molecule contained  
213 in the dry matter has to be taken into account for water. This exchange, known as chemical

214 exchange, is one of the most efficient mechanisms of water relaxation (Belton, 1987; Hills,  
215 1989b; a; Belton, 1990; Denisov, 2002). Consequently, water relaxation is always sensitive to  
216 water content and its value decreases with water content, explaining the more rapid decrease  
217 in the CPMG signal observed for the driest sample. The same mechanisms are also involved  
218 in the  $T_1$  relaxation from the Saturation Recovery NMR sequence. The intensity measured at  
219 2 s was lower for the driest sample and the recovery of the signal (shorter  $T_1$ ) was faster for  
220 the driest sample.

221 The spin-spin relaxation distributions ( $T_2$ ) from MEM obtained from fitting the CPMG curve  
222 are presented in Figure 3. For all samples, two or three peaks were extracted from the signal  
223 according to the sample dry matter. Two mechanisms can be proposed to explain such multi-  
224 exponential relaxation behaviour. The first is based on the assumption of the chemical  
225 composition of the sample. For example, in the case of the water and fat mixture in an  
226 emulsion, a specific exponential can be attributed to each phase, *i.e.* water and fat (Duval,  
227 2006). However, since our samples were mainly composed of water, this hypothesis did not  
228 hold. The second mechanism is based on the sample microstructure which may induce non-  
229 homogeneous water distribution on a microscopic length scale. Indeed, when water exchange  
230 by diffusion between different compartments is slow compared to the relaxation time value,  
231 the averaging effect is not sufficient to yield a single relaxation time value, and several peaks  
232 are observed for the water relaxation. This multi-exponential relaxation for water has already  
233 been reported for many samples which exhibited restriction to the water diffusion. For  
234 example three peaks have been reported from the relaxation decay curve of vegetable tissues.  
235 These peaks were attributed to water in the vacuole, in the cytoplasm and in the cell wall,  
236 respectively (Snaar, 1992; Van Dusschoten, 1995; Duval, 2005; Musse, 2009). This  
237 mechanism therefore seems the most relevant to explain the multi-exponential behaviour of  
238 the relaxation.

239 For the sludge, depending on the dry matter, two or three peaks were extracted from the signal  
240 (Figure 3-a). Their  $T_2$  values covered a range from 5 to 60 ms. The sludge was composed of  
241 flocculated bacteria which induced heterogeneity in the water distribution. Indeed, water was  
242 always present in bacteria, in and around the flocs. Since water protons are thus in three  
243 different compartments, it is tempting to associate each relaxation time with a water  
244 compartment. Granular sludges have already been studied by NMR (Lens, 1997; Lens, 1999),  
245 and a relaxing agent was used to lower the proton relaxation times in the solution. Relaxation  
246 times of 10-15 ms and 30 ms were attributed to methanogenic (Lens, 1999) and sulfidogenic  
247 bacteria (Lens, 1997), respectively. Water in the granular matrix had a relaxation time of 40-  
248 100 ms (Lens, 1999). According to these results, the first peak could be related to the bacteria  
249 and the second to the water around the bacteria (Figure 3-a). However, a water proton from  
250 the solution could well contribute to the first or the second peak. Since no peak was found  
251 with a value close to the free water value (1.5-3 s), this means that there were some molecules  
252 in the sludge solution that lowered the overall relaxation of the proton of this compartment.  
253 The polymer added for the flocculation could explain the decrease in the water relaxation  
254 time, but the effect of the iron chloride (used to dehydrate the sludge) has also to be taken into  
255 account.

256 Wood relaxation is well documented in the literature (Hsi, 1977; Menon, 1987; Araujo, 1992;  
257 Araujo, 1994; Hartley, 1994; Xu, 1996). Three main relaxation times were found related to  
258 water in cell wall fibrils (fast  $T_2$ ), water in the ray and late wood tracheid lumens (medium  $T_2$ )  
259 and water in early wood tracheid lumens (fast  $T_2$ ). Above the fiber saturation point (FSP),  
260 wood relaxation times are relatively constant over a wide range of water content (Menon,  
261 1987). Below FSB, the relaxation times are a function of water content. The wood used in this  
262 study had a similar relaxation time distribution (Figure 3-b) as that reported for Western Red  
263 Cedar sapwood (Menon, 1987). At a water content of 55%, the mean relaxation times were 10

264 ms, 35 ms and 115 ms. The last two peaks were broad. Wood relaxation is sensitive to cell  
265 size and wood species. Since the wood used in this study was heterogeneous in origin, this  
266 would explain the peak shapes.

267 In a wood and sludge mixture there was water equilibrium between the two. After mixing, the  
268 sludge tended to loose water and the wood tended to gain water. Three typical relaxation  
269 distributions of wood and sludge mixtures are presented in Figure 3-c. The dry matter  
270 mixtures were 24%, 50% and 71%, respectively. Two or three peaks could be seen, the first  
271 being narrow (in the range of 0-10 ms), and the second peak broad, the range becoming larger  
272 with the increase in water content. Eventually, two broad peaks could be seen for the wettest  
273 samples. For the driest samples, the wood FSP was most probably not reached since no  
274 relaxation times were found above 40 ms. When the samples became wetter, the wood water  
275 content must have been above the FSP. Water filled the wood cells and then the relaxation  
276 time distribution could become broader. One important result in this study was that most of  
277 the  $T_2$  relaxation distributions for wood and sludge were in the same range. Thus it was not  
278 possible to distinguish specific NMR signals from the sludge and the wood in the wood-  
279 sludge relaxation distribution.

280

281 Using the Levenberg-Marquardt algorithm to fit the  $T_2$  relaxation decay curves, the smallest  
282 residues were obtained with a three component fitting equation (equation 1). The three  $T_2$   
283 values were consistent with the  $T_2$  distribution discussed above. Relaxation rates ( $R_2 = 1/T_2$ )  
284 for the three components are plotted on Figure 4 for sludge samples (a) and for sludge and  
285 wood mixtures (b). For all samples, a constant decrease was observed with the increase in  
286 water mass over dry matter mass. Moreover, the variation in relaxation rate was the same for  
287 the three components. This demonstrates that all fractions were in equilibrium and were  
288 affected by the dehydration process in the same way, despite the micro heterogeneity in the

289 water distribution in the sample. It should be noted that the same variation was observed for  
290 sludge dehydrated by air drying and by exchange with dry wood. These results confirm that  
291 the main effect on the water relaxation rate in the two samples was the dry matter content.  
292 Spin-lattice relaxation times ( $T_1$ ) were measured for wood and sludge mixtures. As for the  
293 spin-spin relaxation curves, the spin-lattice relaxation curves were fitted with MEM and the  
294 Levenberg-Marquardt algorithm (equation 2). The MEM distributions were composed of two  
295 or three peaks (Figure 5-a), the first peak being narrow (range 5-20 ms), the other peaks being  
296 broad (ranging from 15 ms to 250 ms). The Levenberg-Marquardt algorithm had the smallest  
297 residues for the three components. The difference between the two fitting methods obtained  
298 for some mixtures (two components from MEM and three from the discrete method) is  
299 explained by the wide distribution of the second peak. Indeed, this effect is known to induce  
300 discrepancies between the fitting methods (Mariette, 1996). The second peak obtained by  
301 MEM was decomposed into two discrete  $T_1$  values with the discrete method. As for  $R_2$ , a  
302 linear relationship in a log-log plot was observed between the spin-lattice relaxation rate  $R_1$   
303 and the water mass over dry matter mass (Figure 5-b). Moreover, this relationship was  
304 obtained for the three components. Only the  $T_2$  sensitivity to water content will be considered  
305 for the following MRI measurement.

306

### 307 3.2 MRI

308 Two experimental cells were scanned with the whole body MRI scanner at different periods  
309 of biodegradation. In the mean time, the cells were monitored for biodegradation through  
310 respirometry measurements (Figure 6). Indeed, oxygen consumption is a good indicator of  
311 sludge biodegradation. The respirometric profiles obtained, that were similar for the two cells,  
312 are typical. The oxygen uptake rate increased quickly due to biodegradation of the most easily  
313 biodegradable substrate. Then, when all this matter had been degraded, a break in the

314 exponential growth was observed. The oxygen consumption rate then decreased until all the  
315 biodegradable substrates had completely disappeared. During this decrease, the slowly  
316 biodegradable organic matter was hydrolysed before being consumed by micro-organisms.  
317 After 27 days, consumption rate returned to ground state and respirometric study could then  
318 be stopped (Tremier, 2005; Berthe, 2007).

319 Both respirometric cells were thus scanned at D0 before biodegradation, then cell 1 at D3  
320 after the biodegradation peak, and finally cell 2 at D27 when biodegradation was low and  
321 constant. Examples of MR images at D0, D3 and D27 are presented in Figure 7. Images (a)  
322 and (b) and images (c) and (d) were taken at the same location in cell 1 and in cell 2,  
323 respectively. At D0, cell 1 (Figure 7-a) and cell 2 (Figure 7-c) images were similar: no  
324 differences between the MR images for the two cells could be seen. The wet pieces of wood  
325 covered with sludge were clearly visible. The black areas were the air space between the  
326 bulking agents. The contrast in the image will allow to implement image segmentation  
327 method to compute the inter porosity and the specific surface area. For larger pieces of wood,  
328 the edges of the wood tended to be more intense than the centres, showing that the water had  
329 not yet fully hydrated the centres of the wood. NMR relaxation experiments showed that this  
330 process required at least 10h (data not shown). After 3 days, the edge effect was less visible  
331 for cell 1 and the wood chips were even better defined (Figure 7-b). MR images of cell 2  
332 taken after 27 days were highly contrasted. The MR image (Figure 7-d) showed two distinct  
333 areas. Very low signal intensity was detected at the bottom of the image, compared with a  
334 high level signal intensity at the top. This was due to the fact that cell 2 became highly  
335 heterogeneous in water content in 27 days. The low intensity area had dry matter content of  
336 around 60-70%. The intensity of the mixture signal was too low to be fully detected with  
337 MRI. The other area had a dry matter content of around 25%, which demonstrated water  
338 transfer in the cell. At D3, the water content in cell 1 also began to be inhomogeneous, but to

339 a lesser extent. The average dry matter content was 44%, two percent less than at D0. The  
340 contrast between D3 and D27 was thus due to the difference in dry matter content.

341 MRI images were obtained with a spin echo sequence, the grey level intensities being a  
342 function of both relaxation times ( $T_1$ ,  $T_2$ ) and the amount of water (see eq.3). Since the  
343 repetition time,  $T_R$ , was 1 s and the largest spin-lattice relaxation time ( $T_1$ ) found for the

344 wettest wood and sludge mixture was 250 ms, then in equation 3,  $\left(1 - \beta e^{-\frac{T_R}{T_1}}\right) \sim 1$ . Thus, the

345 MR images were not  $T_1$  weighted. Equation 3 can be rewritten for the three components as:

$$346 \quad S_{ES} = I_1 e^{-\frac{T_E}{T_{21}}} + I_2 e^{-\frac{T_E}{T_{22}}} + I_3 e^{-\frac{T_E}{T_{23}}} \quad \text{Eq.4}$$

347

348 Since the intensity of each component  $I_i$  and the three  $T_2$  relaxation times were strongly  
349 dependent on the water content of the sample, the global signal intensity should consequently  
350 also be directly related to water content in the mixture. This direct relationship was checked  
351 by taking samples from cell 1 at D3 and from cell 2 at D27 at different heights in the cells  
352 where MR images showed inhomogeneity. NMR and moisture content measurements were  
353 performed on these samples. Signal intensities at 8 ms were extracted from the NMR CPMG  
354 experiments and plotted against dry matter (Figure 8). As expected, the intensities decreased  
355 with dry matter content. Despite the biological activity during the 27 days of storage, no  
356 biodegradation effect was observed. The results provide evidence that the effect of biological  
357 activity on the NMR signal of wood and sludge mixtures is negligible with regard to dry  
358 matter content. The decay was non-linear. Indeed, with an 8 ms echo time, the multi-  
359 exponential behaviour introduced a weighting from the different components. We  
360 demonstrated that the grey levels of the MRI images were directly related to dry matter  
361 content when the water content was above 40-30%. Below this value the signal was too low  
362 to be detected with this MRI protocol.



363 MRI has been used previously to monitor wood decay by fungus (Muller, 2002): indeed  
364 biological activity means a local increase in water content, which leads to a local change in  
365 relaxation times and intensities. In this experiment, respirometry showed that biodegradation  
366 occurred and both the NMR measurements and the MR images showed changes in the dry  
367 matter content. MR images gave 3D representation of the heterogeneity of dry matter content  
368 in the cells after 27 days of biodegradation (Figure 9). Heterogeneity was both vertical and  
369 horizontal. Biodegradation may contribute to the heterogeneity of the dry matter, but the main  
370 cause seems to be related to the cell design. The dried area is above the tube where air flows  
371 into the cell. The air rate must be too fast and then has a drying effect. The humid area is  
372 located under the tube where air flows out of the cell (Figure 2). Even with the water trap,  
373 some water seems to condense in this tube and then drops to the wood and sludge mixture.  
374 Thus, these MR images cannot be taken as proof of biodegradation activity. Nevertheless,  
375 they will be used to improve the design of the respiratory cell.

#### 376 **4. Conclusion**

377 We have shown that the NMR water relaxation for wood and sludge exhibited a multi-  
378 exponential relaxation time behaviour which can be explained by the microstructure of the  
379 matrix. Moreover, a high dry matter content effect on the relaxation was observed for sludge  
380 samples and for sludge and wood mixtures. This effect was the same whatever the relaxation  
381 time component, which confirmed that the dry matter content had the main effect on the NMR  
382 parameters. Wood and sludge mixtures were scanned successfully by MRI using a spin echo  
383 sequence. The grey level intensities were correlated with the dry matter content, thus  
384 demonstrating the feasibility of MRI to quantify the water distribution in respiratory cells.  
385 Moreover, image resolution was good enough for image analysis. Since voxel size was much  
386 smaller than pore volume, porosity and specific surface area should be available.

387

388 **Acknowledgments**

389 The authors thank Mylene Launay and Mireille Cambert for their technical assistance.

390

391 **Figure legends**

392 Figure 1 : Diagram of respirometric apparatus

393

394 Figure 2 : Typical CPMG (a) and SR (b) decay curves for two ratios of sludge and wood with  
395 70 % (■) and 24 % (◆) dry matter.

396

397 Figure 3 : Spin-spin relaxation time ( $T_2$ ) distributions. Adjustments were made with the MEM  
398 routine. (a) Sludge samples with 15%, 25% and 52% dry matter content (b) Wet wood with  
399 dry mater of 45% (c) Mixtures of sludge and wood with 24.2%, 50.2% and 70.8% dry matter  
400 content. One used the CPMG sequence (3000 echoes, with  $\tau = 0.1$  ms,  $RD = 2$  s,  $NS = 8$ ).

401

402 Figure 4 : Three component spin-spin relaxation rates ( $1/T_2=R_2$ ) for (a) sludge samples and  
403 (b) sludge and wood mixtures at various water over DM mass ratios. **First component (◆),**  
404 **second component (■) and third component (▲).** One used the CPMG sequence (3000  
405 echoes, with  $\tau = 0.1$  ms,  $RD = 2$  s,  $NS = 8$ ). Dashed lines  $\propto(m_W/m_{DM})^{-1}$  are to assist reading.

406

407 Figure 5 : Spin-lattice relaxation time ( $T_1$ ) distributions for mixtures of sludge and wood with  
408 24.2% and 70.1% dry matter content (a). Adjustments were made with the MEM routine.

409 Three component spin-lattice relaxation rates ( $R_1$ ) for sludge and wood mixtures at various  
410 water over DM mass ratios (b). First component (◆), second component (■) and third  
411 component (▲).One used the SR sequence (100 points with  $\tau_1=5$  ms,  $\tau_{100}= 2000$  ms,  $RD = 2$   
412 s,  $NS = 8$ ). Dashed lines  $\propto(m_W/m_{DM})^{-1}$ to assist reading.

413

414 Figure 6 : Oxygen uptake rate over time for the two respirometric cells used in the combined  
415 MRI-Respirometry set up.

416

417 Figure 7 : MRI images of respirometric cells 1 and 2 taken with a spin echo sequence ( $T_E = 8$   
418 ms,  $T_R = 1000$  ms, FOV = 220 mm x 220 mm, thickness 2mm, sampling 256x256): Cell 1 at  
419 D0 (a) and D3 (b), Cell 2 at D0 (c) and D27 (d).MR images were representative of the area 3  
420 cm below the centre of the airtight cylindrical reactor.

421

422 Figure 8 : Spin-spin relaxation intensities normalised by sample mass extracted from CPMG  
423 decay curves at 8 ms compared to dry matter content of sludge and wood mixtures. Samples  
424 were taken from the leftover mixture at D0 and at D3 and D27 from the respirometric cell 1  
425 and cell 2, respectively. One used the CPMG sequence (3000 echoes, with  $\tau=0.1$ ms,  
426 RD=2s, NS=8).

427

428 Figure 9 : MRI images of respirometric cell 2 at D27, taken with a spin echo sequence ( $T_E =$   
429 8 ms,  $T_R = 1000$  ms, FOV = 220 mm x 220 mm, thickness 2mm, sampling 256x256).  
430 Selected images were separated by 3.6 cm. They are labelled from the bottom (slice 1) to the  
431 top (slice 45) of the cell.

432

434 **References**

- 436 Adani, F., Lozzi, P., Genevini, P., 2001. Determination of biological stability by oxygen  
437 uptake on municipal solid waste and derived products. *Compost Science & Utilization*  
438 9, 163-178.
- 439 Agnew, J.M., Leonard, J.J., 2003. The physical properties of compost. *Compost Science &*  
440 *Utilization* 11, 238-264.
- 441 Annan, J.S., White, R.K. 1998 Evaluation of techniques for measuring air filled porosity in  
442 composts of municipal biosolids and wood chips. *In* Conference of composting in the  
443 southeast, September 9-11, Athens, Georgia, USA.
- 444 Araujo, C.D., Avramidis, S., Mackay, A.L., 1994. Behaviour of Solid Wood and Bound  
445 Water as a Function of Moisture Content a Proton Magnetic Resonance Study.  
446 *Holzforschung* 48, 69-74.
- 447 Araujo, C.D., Mackay, A.L., Hailey, J.R.T., Whittall, K.P., Le, H., 1992. Proton Magnetic-  
448 Resonance Techniques for Characterization of Water in Wood - Application to White  
449 Spruce. *Wood Science and Technology* 26, 101-113.
- 450 Belton, P.S. 1990 Can Nuclear Magnetic Resonance Give Useful Information About the State  
451 of Water in Foodstuffs? *Comments on Agricultural and Food Chemistry Science*  
452 2,179-209..
- 453 Belton, P.S., Hills, B.P., 1987. The effects of diffusive exchange in heterogeneous systems on  
454 N.M.R line shapes and relaxation processes. *Molecular Physics* 61, 999-1018.
- 455 Berthe, L., Druilhe, C., Massiani, C., Tremier, A., de Guardia, A., 2007. Coupling a  
456 respirometer and a pycnometer, to study the biodegradability of solid organic wastes  
457 during composting. *Biosystems Engineering* 97, 75-88.
- 458 Bonn, D., Rodts, S., Groenink, M., Rafai, S., Shahidzadeh-Bonn, N., Coussot, P., 2008. Some  
459 applications of magnetic resonance imaging in fluid mechanics: Complex flows and  
460 complex fluids. *Annual Review of Fluid Mechanics* 40, 209-233.
- 461 Brownstein, K.R., Tarr, C.E., 1979. Importance of classical diffusion in NMR studies of water  
462 in biological cells. *Physical Review A* 19, 2446-2453.
- 463 Butz, P., Hofmann, C., Tauscher, B., 2005. Recent developments in noninvasive techniques  
464 for fresh fruit and vegetable internal quality analysis. *Journal of Food Science* 70,  
465 R131-R141.
- 466 Denisov, V.P., Halle, B., 2002. Hydrogen exchange rates in proteins from water H-1  
467 transverse magnetic relaxation. *Journal of the American Chemical Society* 124,  
468 10264-10265.
- 469 Duval, F., Cambert, M., Mariette, F., 2005. NMR study of tomato pericarp tissue by spin-spin  
470 relaxation and water self-diffusion. *Applied Magnetic Resonance* 28, 29-40.
- 471 Duval, F.P., Van Duynhoven, J.P.M., Bot, A., 2006. Practical implications of the phase-  
472 compositional assessment of lipid-based food products by time-domain NMR. *Journal*  
473 *of the American Oil Chemists' Society* 83, 905-912.
- 474 Faure, P., Care, S., Po, C., Rodts, S., 2005. An MRI-SPI and NMR relaxation study of drying-  
475 hydration coupling effect on microstructure of cement-based materials at early age.  
476 *Magnetic Resonance Imaging* 23, 311-314.
- 477 Gea, T., Barrena, R., Artola, A., Sanchez, A., 2004. Monitoring the biological activity of the  
478 composting process: Oxygen uptake rate (OUR), respirometric index (RI), and  
479 respiratory quotient (RQ). *Biotechnology and Bioengineering* 88, 520-527.

- 480 Grenier, A., Lucas, T., Collewet, G., Le Bail, A., 2003. Assessment by MRI of local porosity  
481 in dough during proving. Theoretical considerations and experimental validation using  
482 a spin-echo sequence. *Magnetic Resonance Imaging* 21, 1071-1086.
- 483 Gupta, R., Garg, V.K., 2008. Stabilization of primary sewage sludge during vermicomposting.  
484 *Journal of Hazardous Materials* 153, 1023-1030.
- 485 Hartley, I.D., Kamke, F.A., Peemoeller, H., 1994. Absolute Moisture Content Determination  
486 of Aspen Wood Below the Fiber Saturation Point Using Pulsed NMR. *Holzforschung*  
487 48, 474-479.
- 488 Haug, R.T., 1993. *The practical handbook of composting engineering*. Lewis Publishers, Boca  
489 Raton, Florida, USA.
- 490 Hills, B., 1998. *Magnetic resonance imaging in food science*. A Wiley Interscience  
491 publication, New York, USA.
- 492 Hills, B.P., Takacs, S.F., Belton, P.S., 1989a. The effects of proteins on the proton NMR  
493 transverse relaxation time of water. II protein aggregation. *Molecular Physics* 67, 919-  
494 937.
- 495 Hills, B.P., Takacs, S.F., Belton, P.S., 1989b. The effects of proteins on the proton NMR  
496 transverse relaxation times of water. I Native bovine serum albumine. *Molecular*  
497 *Physics* 67, 903-918.
- 498 Hsi, E., Hossfeld, R., Bryant, R.G., 1977. Nuclear magnetic resonance relaxation study of  
499 water absorbed on milled northern white-cedar. *Journal of Colloid and Interface*  
500 *Science* 62, 389-395.
- 501 Iannotti, D.A., Grebus, M.E., Toth, B.L., Madden, L.V., Hoitink, H.A.J., 1994. Oxygen  
502 Respirometry to Assess Stability and Maturity of Composted Municipal Solid-Waste.  
503 *Journal of Environmental Quality* 23, 1177-1183.
- 504 Lens, P., Pol, L.H., Lettinga, G., Van As, H., 1997. Use of  $H^1$  NMR to study transport  
505 processes in sulfidogenic granular sludge. *Water Science and Technology* 36, 157-  
506 163.
- 507 Lens, P., Vergeldt, F., Lettinga, G., Van As, H., 1999.  $H^1$  NMR characterisation of the  
508 diffusional properties of methanogenic granular sludge. *Water Science and*  
509 *Technology* 39, 187-194.
- 510 Lucas, T., Grenier, A., Quellec, S., Le Bail, A., Davenel, A., 2005. MRI quantification of ice  
511 gradients in dough during freezing or thawing processes. *Journal of Food Engineering*  
512 17, 98-108.
- 513 Mantle, M.D., Sederman, A.J., 2003. Dynamic MRI in chemical process and reaction  
514 engineering. *Progress in Nuclear Magnetic Resonance Spectroscopy* 43, 3-60.
- 515 Mariette, F., 2004. NMR relaxometry and MRI techniques: a powerful association in food  
516 science. *Comptes Rendus Chimie* 7, 221-232.
- 517 Mariette, F. 2006 NMR imaging of dairy products. *Modern Magnetic Resonance, Part 3:*  
518 *Applications in Materials Science and Food Science*, Springer; London, UK
- 519 Mariette, F., Guillement, J.P., Tellier, C., Marchal, P. 1996 Continuous relaxation time  
520 distribution decomposition by MEM. *In Signal Treatment and Signal Analysis in*  
521 *NMR*, Elsevier, Paris, France.
- 522 Marquardt, D.W., 1963. An algorithm for least squares estimations of nonlinear parameters.  
523 *Journal of the Society for Industrial and Applied Mathematics* 11, 431.
- 524 Meiboom, S.G.D., 1958. Compensation for pulse imperfections in Carr-Purcell NMR  
525 experiments. *Review of Scientific Instruments* 29, 688.
- 526 Menon, R.S., Mackay, A.L., Hailey, J.R.T., Bloom, M., Burgess, A.E., Swanson, J.S., 1987.  
527 An NMR Determination of the physiological water distribution in wood during drying.  
528 *Journal of Applied Polymer Science* 33, 1141-1155.

529 Muller, U., Bammer, R., Teischinger, A., 2002. Detection of incipient fungal attack in wood  
530 using magnetic resonance parameter mapping. *Holzforschung* 56, 529-534.

531 Musse, M., Quellec, C., Devaux, M.F., Cambert, M., Lahaye, M., Mariette, F., 2009. An  
532 investigation of the structural aspects of the tomato fruit by means of quantitative  
533 nuclear resonance imaging. *Magnetic Resonance Imaging* 27, 709-719.

534 Olson, M.S., Ford, R.M., Smith, J.A., Fernandez, E.J., 2004. Quantification of bacterial  
535 chemotaxis in porous media using magnetic resonance imaging. *Environmental  
536 Science & Technology* 38, 3864-3870.

537 Palmowski, L., Müller, J., 2003. Anaerobic degradation of organic materials-significance of  
538 the substrate surface area. *Water Science and Technology* 47, 231-238.

539 Richardson, J.C., Bowtell, R.W., Mader, K., Melia, C.D., 2005. Pharmaceutical applications  
540 of magnetic resonance imaging (MRI). *Advanced Drug Delivery Reviews* 57, 1191-  
541 1209.

542 Sherwood, J.L., Sung, J.C., Ford, R.M., Fernandez, E.J., Maneval, J.E., Smith, J.A., 2003.  
543 Analysis of bacterial random motility in a porous medium using magnetic resonance  
544 imaging and immunomagnetic labelling. *Environmental Science & Technology* 37,  
545 781-785.

546 Snaar, J.E.M., Van As, H., 1992. Probing water compartments and membrane permeability in  
547 plant cells by  $H^1$  NMR relaxation measurements. *Biophysical Journal* 63, 1654-1658.

548 Su, D., McCartney, D., Wang, Q., 2006. Comparison of free air space test methods. *Compost  
549 Science & Utilization* 14, 103-113.

550 Tremier, A., de Guardia, A., Massiani, C., Paul, E., Martel, J.L., 2005. A respirometric  
551 method for characterising the organic composition and biodegradation kinetics and the  
552 temperature influence on the biodegradation kinetics, for a mixture of sludge and  
553 bulking agent to be co-composted. *Bioresource Technology* 96, 169-180.

554 Van Dusschoten, D., De Jager, P.A., Van As, H., 1995. Extracting diffusion constants from  
555 echo-time-dependent PFG NMR data using relaxation-time information. *Journal of  
556 Magnetic Resonance Series A* 116, 22-28.

557 Xu, Y., Araujo, C.D., MacKay, A.L., Whittall, K.P., 1996. Proton spin-lattice relaxation in  
558 wood - T-1 related to local specific gravity using a fast-exchange model. *Journal of  
559 Magnetic Resonance Series B* 110, 55-64.

560 Ziegler, G.R., MacMillan, B., Balcom, B.J., 2003. Moisture migration in starch molding  
561 operations as observed by magnetic resonance imaging. *Food Research International*  
562 36, 331-340.

563  
564  
565  
566  
567  
568  
569

Figure 1

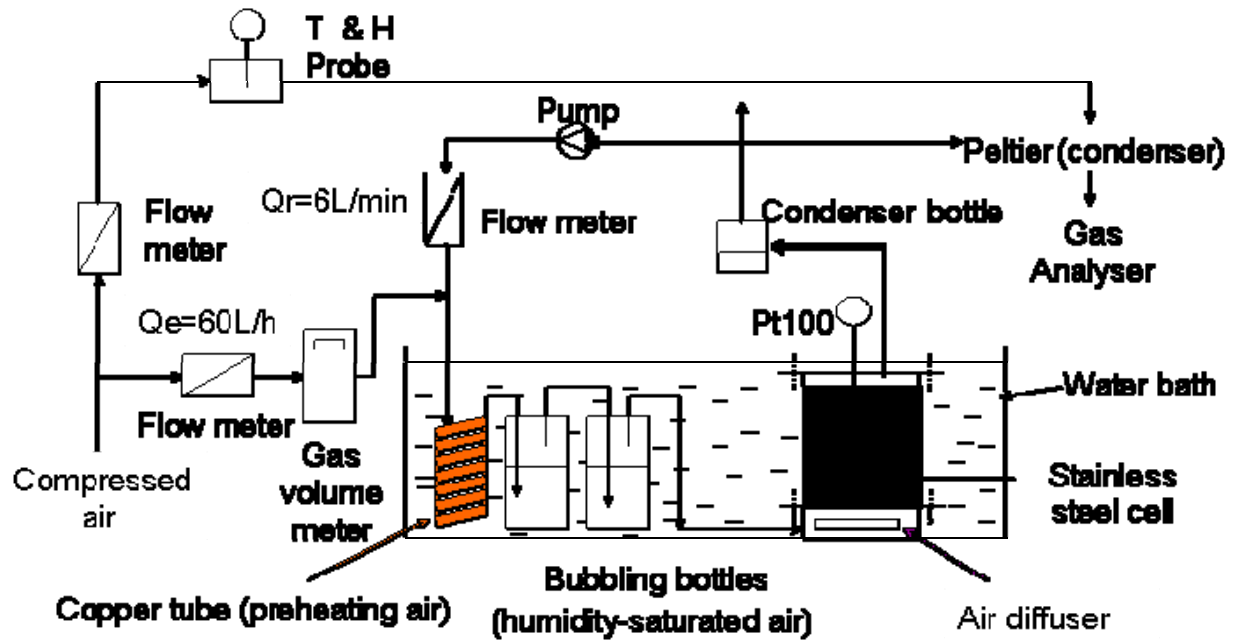




Figure 2

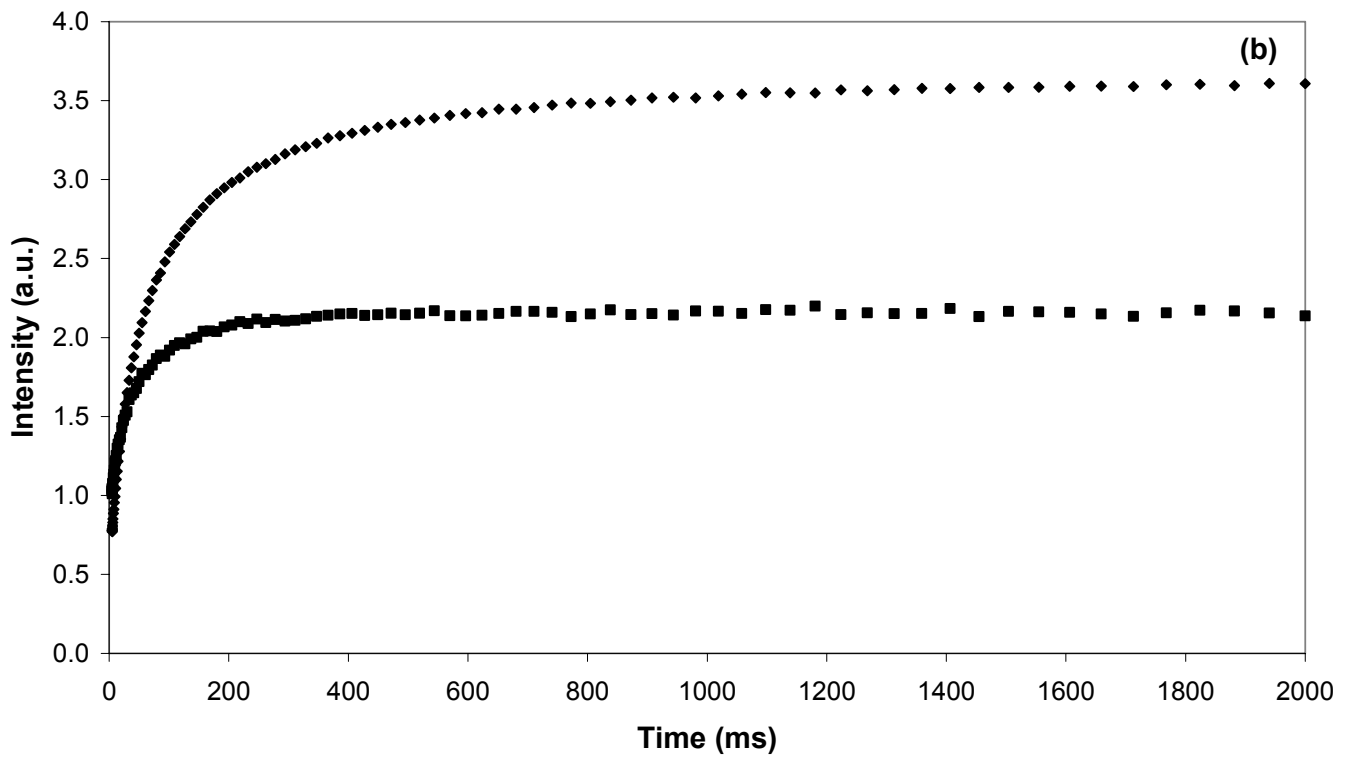
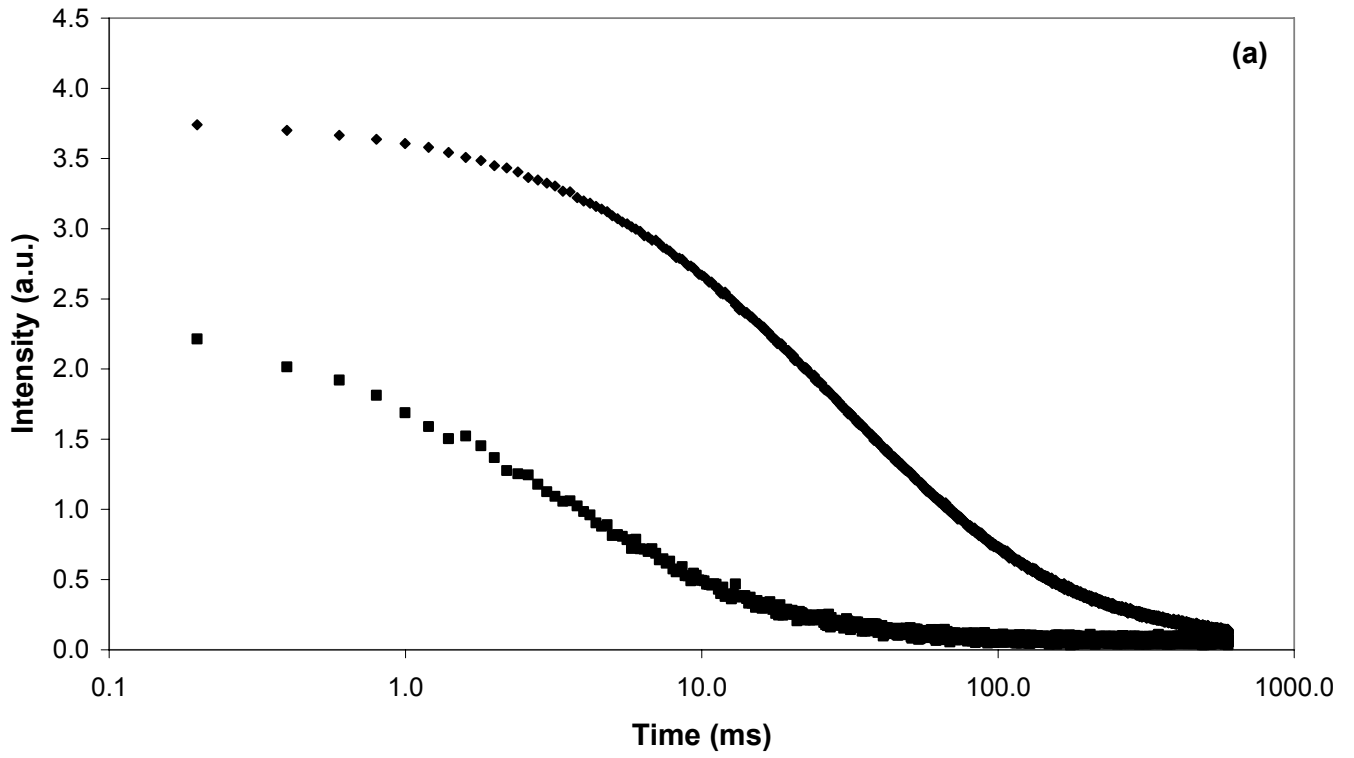


Figure 3

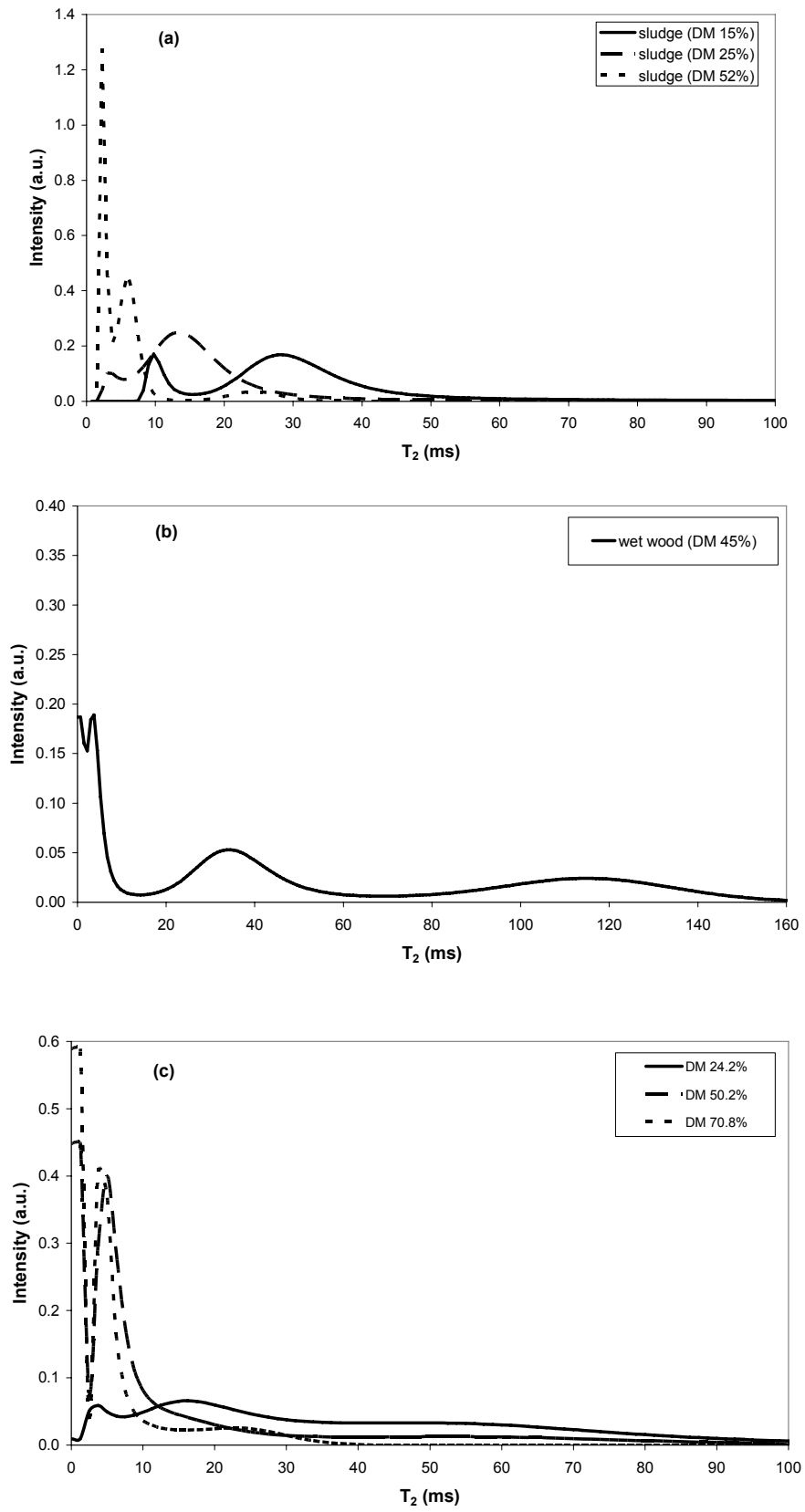


Figure 4

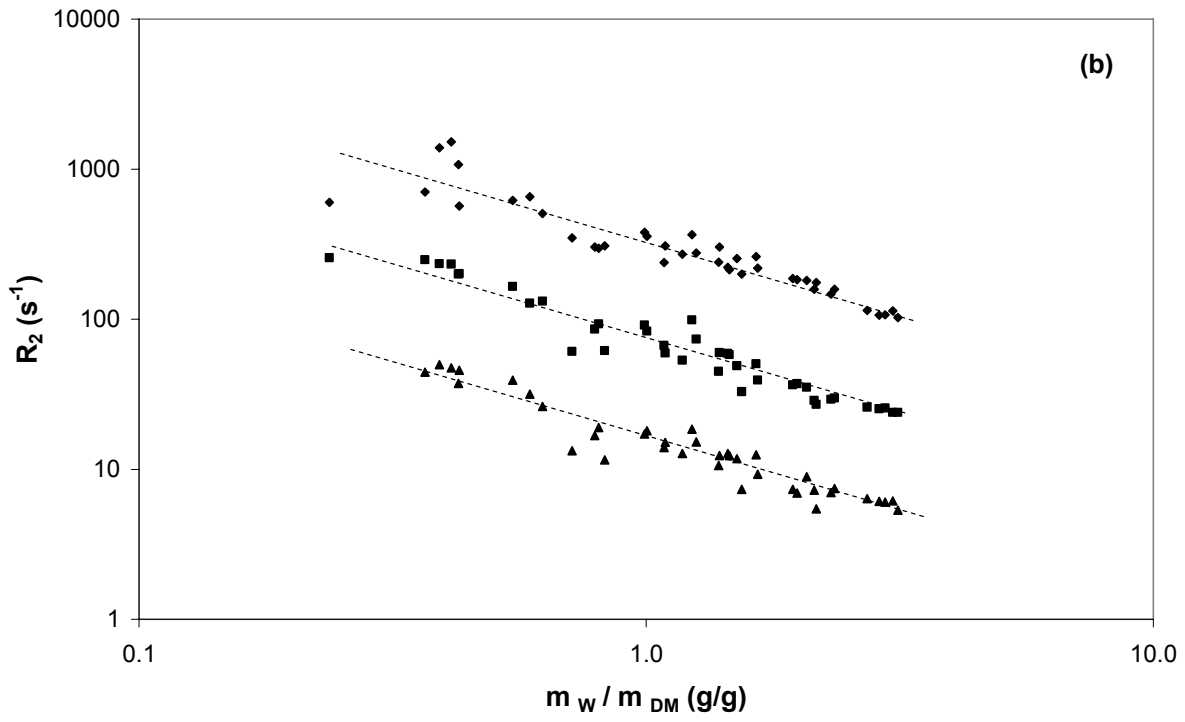
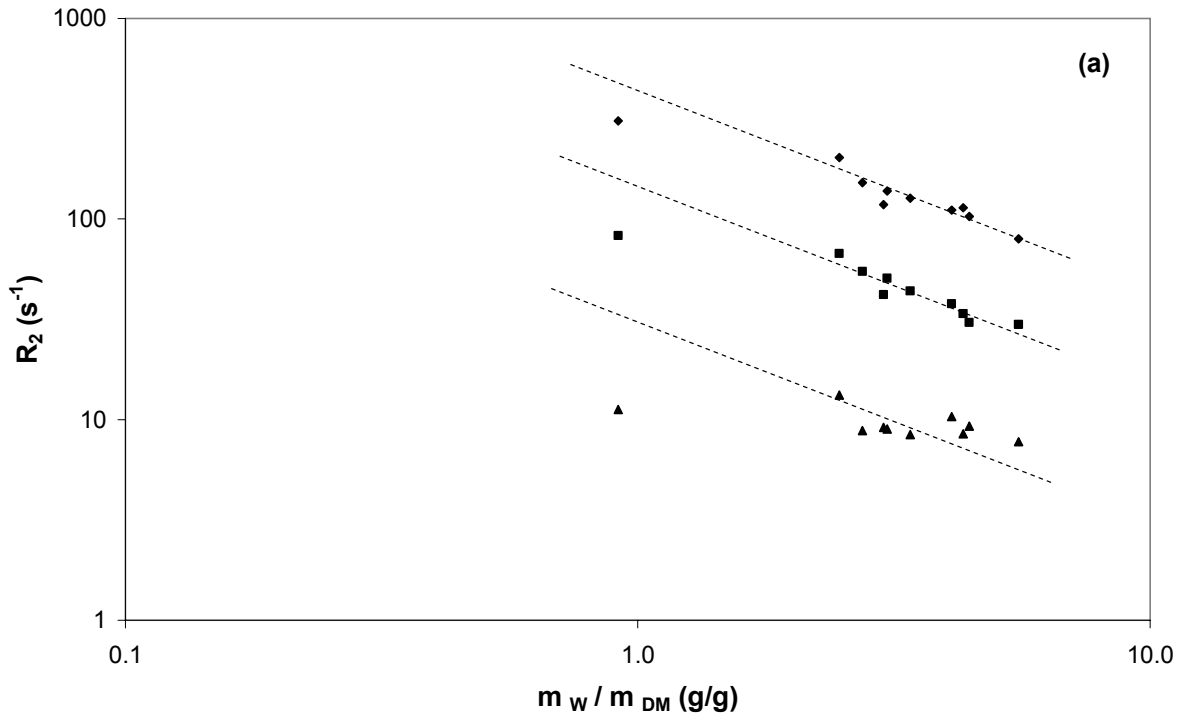


Figure 5

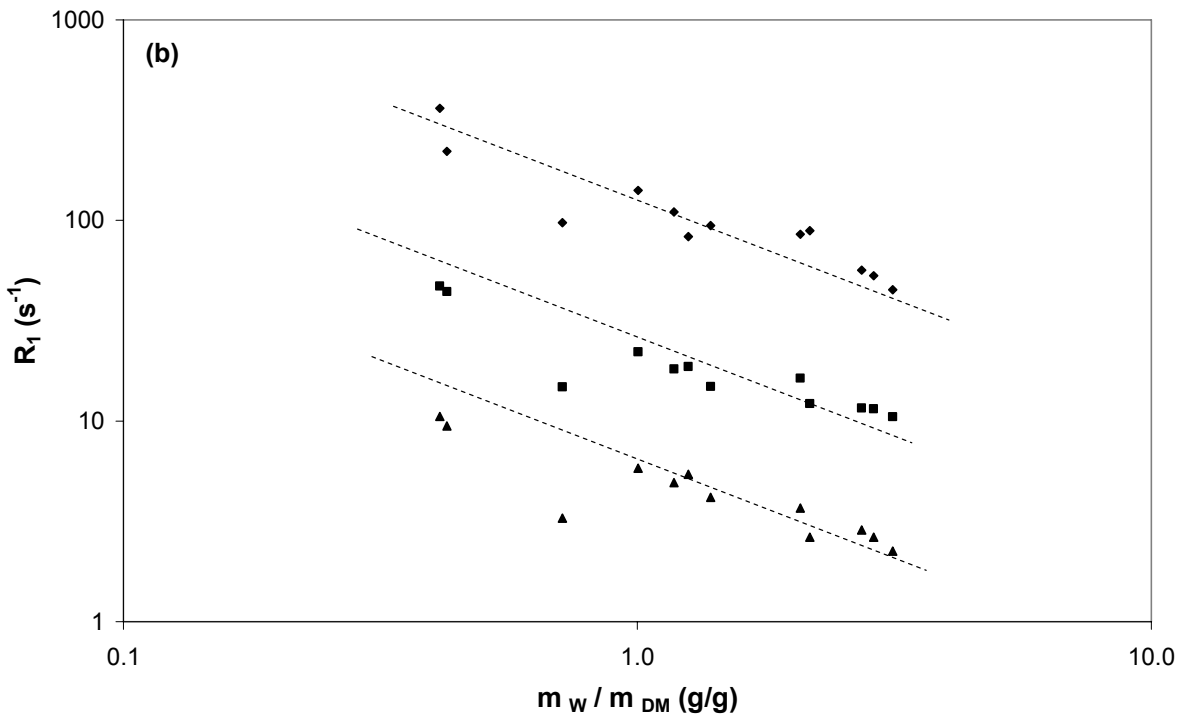
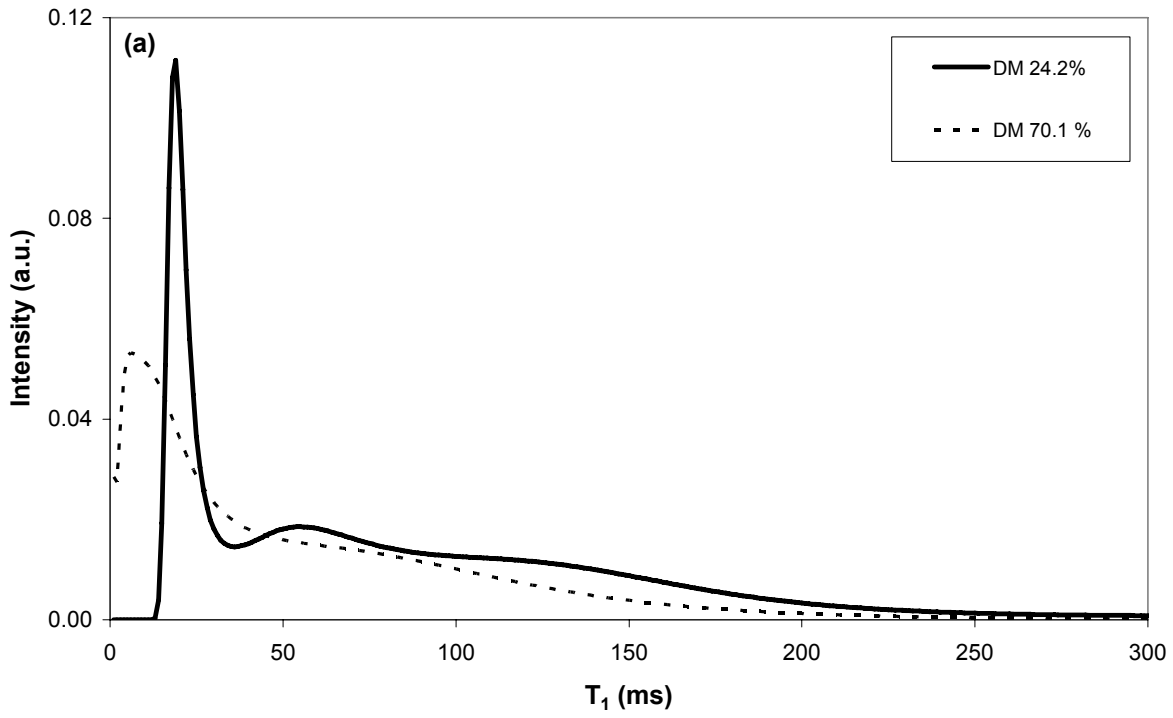


Figure 6

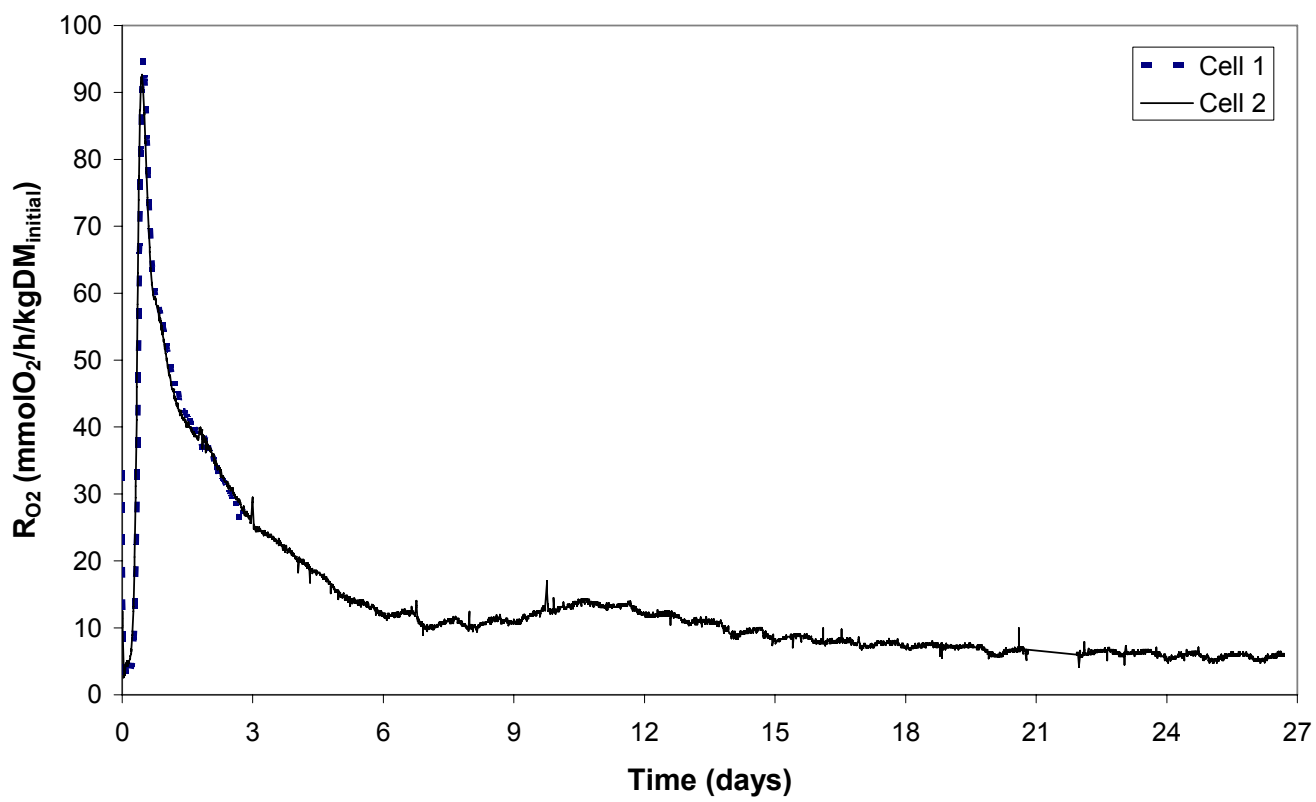


Figure 7

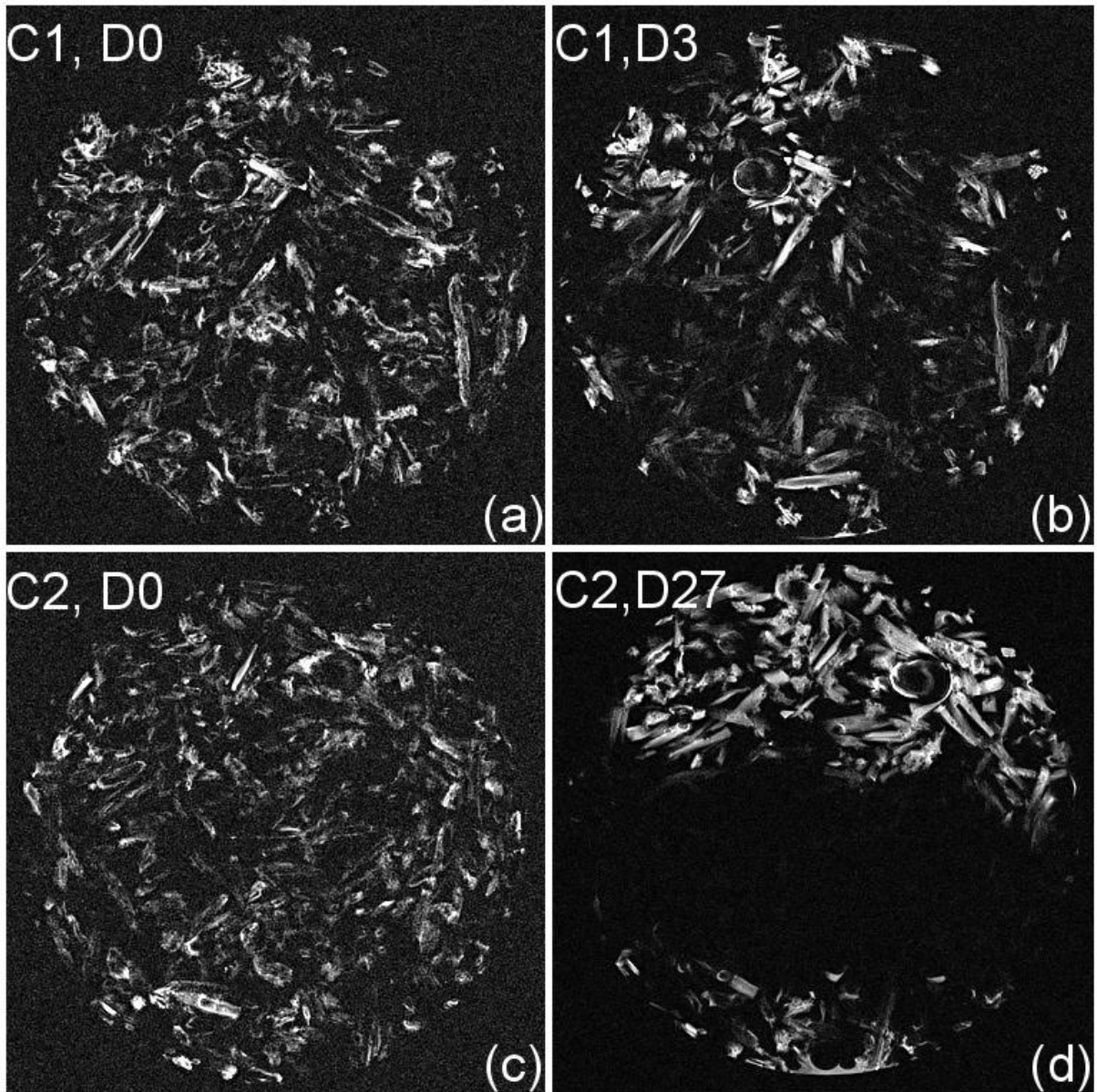


Figure 8

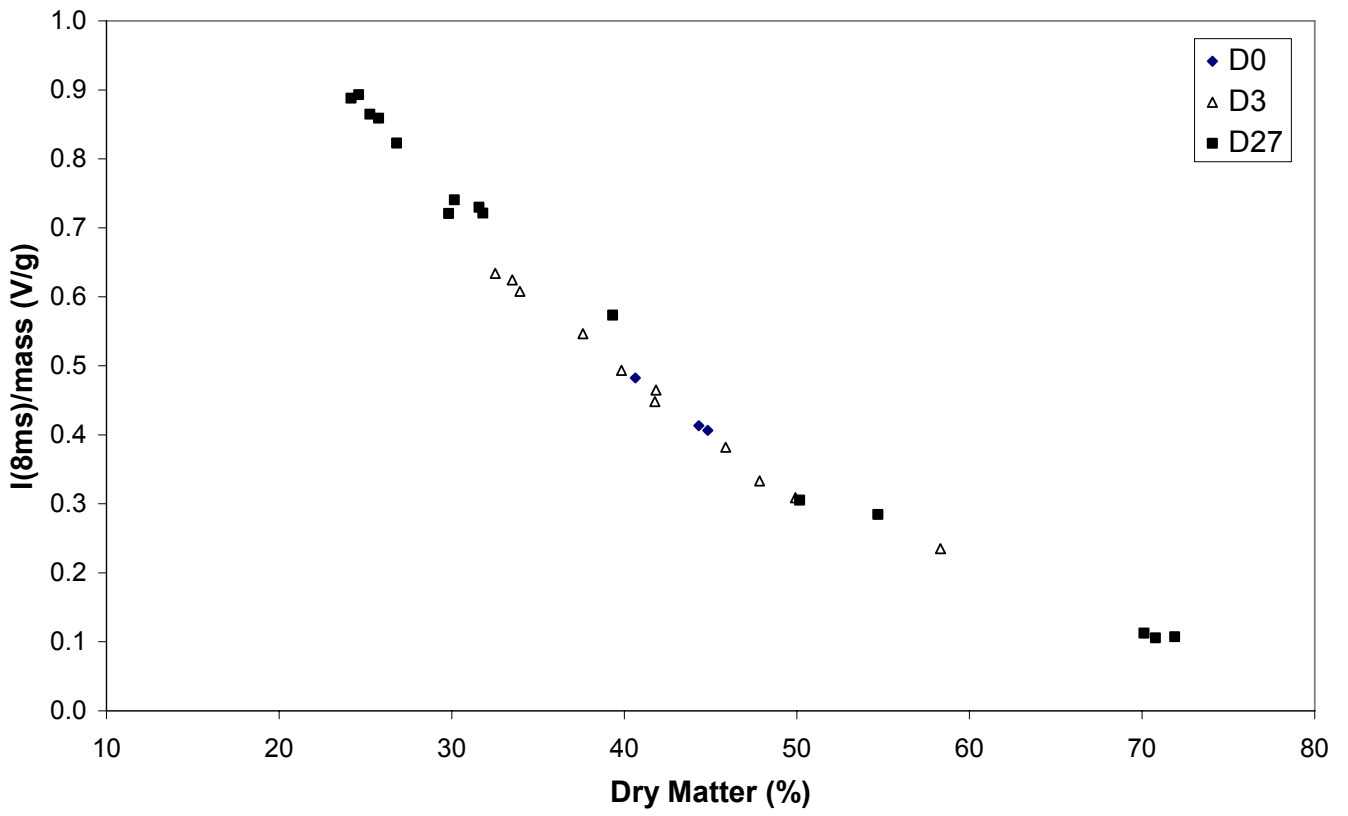


Figure 9

